Conformation-Specific Spectroscopy of Asparagine-Containing Peptides: Influence of Single and Adjacent Asn Residues on Inherent Conformational Preferences

Karl N. Blodgett[a], Joshua L. Fischer[a], Jaeyeon Lee[b], Soo Hyuk Choi[b], and Timothy S. Zwier[a]*

[a]*Department of Chemistry, Purdue University, West Lafayette, Indiana 47907-2084, United States*
[b]*Department of Chemistry, Yonsei University, Seoul 03722, Korea*

Table of Contents

1. **Synthetic Procedure for Ac-Asn-NHBn, Ac-Ala-Asn-NHBn, and Ac-Asn-Asn-NHBn** **p. 3**

2. **R2PI and IR-UV Holeburning Spectra of Ac-Asn-NHBn,** **p. 3-4**

3. **Structural Comparison of Conf A and Conf A^{Rot}, and Relaxed Benzyl Dihedral Potential Energy Scan of the C7$_{eq}$//*C6/C7* Structural Motif of Ac-Asn-NHBn** **p. 5-6**

4. **R2PI and IR-UV Holeburning Spectra of Ac-Ala-Asn-NHBn** **p. 7-8**

5. **R2PI and IR-UV Holeburning Spectra of Ac-Asn-Asn-NHBn** **p. 8-9**

6. **Hydrogen Bonding Cycles, Calculated Distances, and Experimental Vibrational Frequencies for those Interactions Found in the Asn-Containing Peptides, Gln-Containing Peptides, and β-peptide Containing Foldamers** **p. 10-11**

7. **Backbone Overlap, and Hydride Stretch Comparison Spectra, of Ac-Ala-Asn-NHBn and Ac-Asn-Asn-NHBn** **p. 12**

8. **Backbone Overlap of Ac-Ala-Asn-NHBn and** **p. 13**

Ac-Ala-Gln-NHBn

9. Backbone Overlap of Ac-Asn-Asn-NHBn and Ac-Gln-Gln-NHBn **p. 13**

10. Free Energy Corrections for Ac-Asn-NHBn, Ac-Ala-Asn-NHBn, and Ac-Asn-Asn-NHBn **p. 14-17**

11. Energetic Reordering upon Substitution of NHBn cap with NHMe **p. 17-21**

12. Figure S10: Comparison of NHBn and NHMe Capped Ac-Asn-Asn-NHBn Conf A and Calculated Low Energy C10//*C6/C7//*C11 Structures **p. 22**

13. Comparison of Type I β-turn Dihedral Angles of Assigned Dipeptides With Those Found in the Protein Data Bank with Sequence X(AN)X and X(NN)X **p. 23-24**

14. References **p. 25-27**

1. Synthetic Procedure for Ac-Asn-NHBn, Ac-Ala-Asn-NHBn, and Ac-Asn-Asn-NHBn

Reagents and *N*-Cbz-protected α-amino acids were purchased from Sigma-Aldrich and Chem-Impex International. A 0.1 M solution of Cbz-Asn-OH (1 equiv.) and benzylamine (1.1 equiv.) in DMF was added with EDCI (1.5 equiv.) and HOBt (1.3 equiv.). The mixture was stirred at rt for a day, diluted with EtOAc and then washed successively with 10% aqueous citric acid, aqueous saturated $NaHCO_3$ and brine. The organic layer was dried over $MgSO_4$, filtered and concentrated in vacuo. The crude product was purified by flash column chromatography to give Cbz-Asn-NHBn (90%). A mixture of Cbz-Asn-NHBn (1 equiv.), acetic anhydride (1.1 equiv.) and 10% Pd/C (10% w/w) in methanol was stirred under H_2 gas (1 atm, balloon) at rt for 2 h and then filtered through celite pad. The filtrate was concentrated in vacuo to give **1** (82%). Dipeptides **2** and **3** were synthesized from Cbz-Asn-NHBn in three steps by methods analogous to those used for **1**: Cbz deprotection, EDCI-mediated coupling and Cbz deprotection-acetylation. A mixture of Cbz-Asn-NHBn (1 equiv.) and 10% Pd/C (10% w/w) in methanol was stirred under H_2 gas (1 atm, balloon) at rt for 2 h, filtered through celite pad, and concentrated in vacuo. The resulting HCl salt form was coupled with Cbz-Ala-OH (1.0 equiv.) and Cbz-Asn-OH (1.0 equiv.) to give Cbz-Ala-Asn-NHBn (54%) and Cbz-Asn-Asn-NHBn (49%), respectively. Each of the *N*-Cbz-protected dipeptide was converted to the desired *N*-acetyl product **2** (92%) or **3** (73%).

Ac-Asn-NHBn (1) ^{1}H NMR (400 MHz, DMSO-d_6) δ 8.29 (triplet, J = 4 Hz, 1H), 8.04 (d, J = 8 Hz, 1H), 7.31-7.19 (m, 6H), 6.86 (s, 1H), 4.59-4.54 (m, 1H), 4.25 (m, 2H), 2.54-2.36 (m, 2H), 1.84 (s,3H); HRMS m/z calculated for $C_{13}H_{17}N_3NaO_3^+$ $[M+Na]^+$ 286.1162, found 286.1162.

Ac-Ala-Asn-NHBn (2) ^{1}H NMR (400 MHz, DMSO-d_6) δ 8.27-8.23 (m, 2H), 8.16 (t, J = 8 Hz, 1H), 7.43 (s, 1H), 7.29-7.18 (m, 5H), 6.91 (s, 1H), 4.51 (quartet, J = 8 Hz, 1H), 4.32-4.13 (m, 3H), 2.53-2.52 (m, 2H), 1.82 (s, 3H), 1.92-1.17 (m, 3H); HRMS m/z calculated for $C_{16}H_{22}N_4NaO_4^+$ $[M+Na]^+$ 335.1533, found 357.1534.

Ac-Asn-Asn-NHBn (3) ^{1}H NMR (400 MHz, DMSO-d_6) δ 8.50-8.28 (m, 3H), 7.56-7.45 (m, 2H), 7.27-7.24 (m, 5H), 6.96-6.90 (m, 2H), 4.51-4.49 (m, 2H), 4.26 (m, 2H), 2.50-2.31 (m, 4H), 1.83 (s, 3H); HRMS m/z calculated for $C_{17}H_{23}N_5NaO_5^+$ $[M+Na]^+$ 400.1591, found 400.1594.

2. R2PI and IR-UV Holeburning Spectra of Ac-Asn-NHBn

The R2PI and IR-UV holeburning spectra for Ac-Asn-NHBn are shown in **Figure S1.** These spectra were obtained by scanning the UV laser across the S_0-S_1 region in which the NHBn chromophore absorbs (37,500 – 37,820 cm^{-1}). The R2PI spectrum displays two Franck-Condon progressions in ~8 and ~10 cm^{-1} modes, with the largest component transitions appearing at 37,627 and 37,578 cm^{-1}, respectively. IR-UV holeburning spectra, shown in red and blue, reveal that these two sets of peaks are due to two unique conformers, labelled conf. A and conf. B in **Figure S1**. Normal mode analysis of the assigned conformers shows that, in each case, the Franck-Condon active vibration is the twisting of the phenyl ring, causing a modulation of the CCCN dihedral angle.

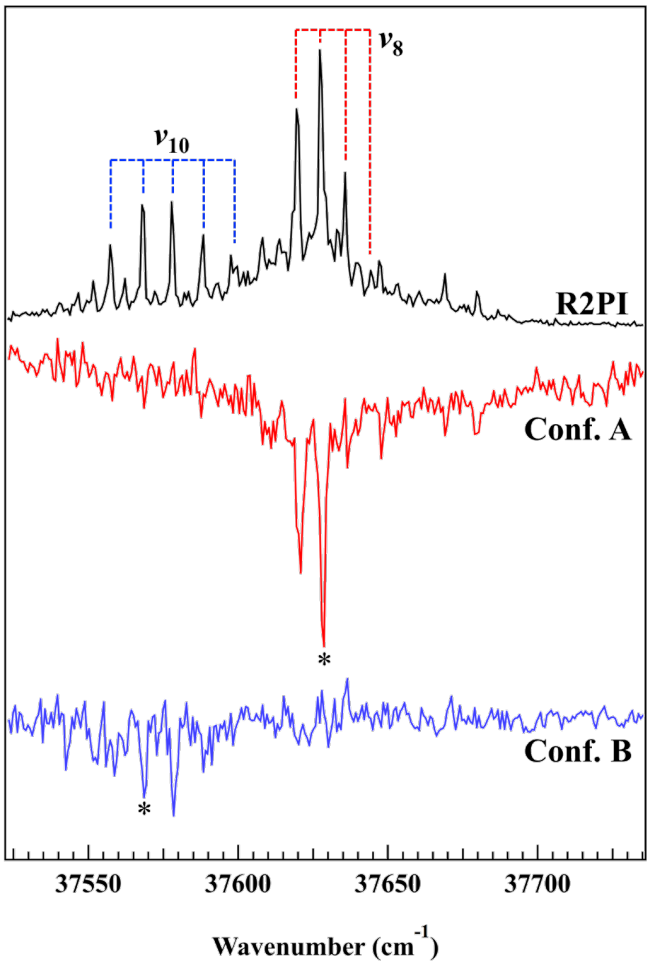

Figure S1: R2PI and IR-UV holeburning spectra of Ac-Asn-NHBn. Peaks marked with an asterisk (37,629 cm^{-1}, Conf. A; 37,569 cm^{-1}, Conf. B) indicate transitions used to collect RIDIR spectra. Vibronic progressions are labeled with tie lines.

3. Structural Comparison of Conf A and Conf A^{Rot}, and Relaxed Benzyl Dihedral Potential Energy Scan of the C7$_{eq}$//*C6/C7* Structural Motif of Ac-Asn-NHBn

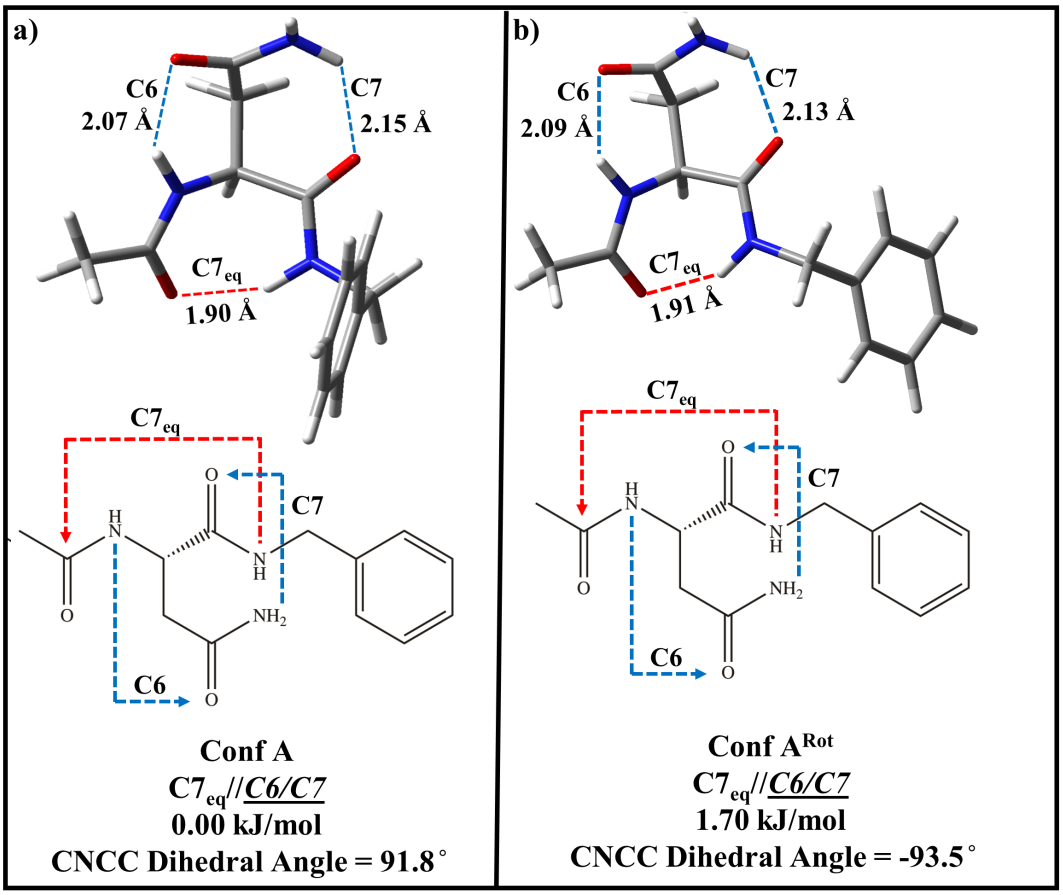

Figure S2: Structures of (a) conformer A and (b) conformer A^{Rot}. 3D structure and 2D hydrogen bonding schematic are presented for each structure, as well as the hydrogen bonding designation, relative zero-point corrected potential energies, and the value of the CNCC dihedral angle, which serves to differentiate the two conformers from one another.

As mentioned in the main text, a possible alternative assignment of conformer B is a benzyl rotamer of conformer A (conf A^{Rot}). **Figure S2** shows a relaxed potential energy scan about the relevant CNCC dihedral angle, indicating where the two minima lie along the potential energy surface. A small (~5 kJ/mol) barrier separates the rotamers from one another.

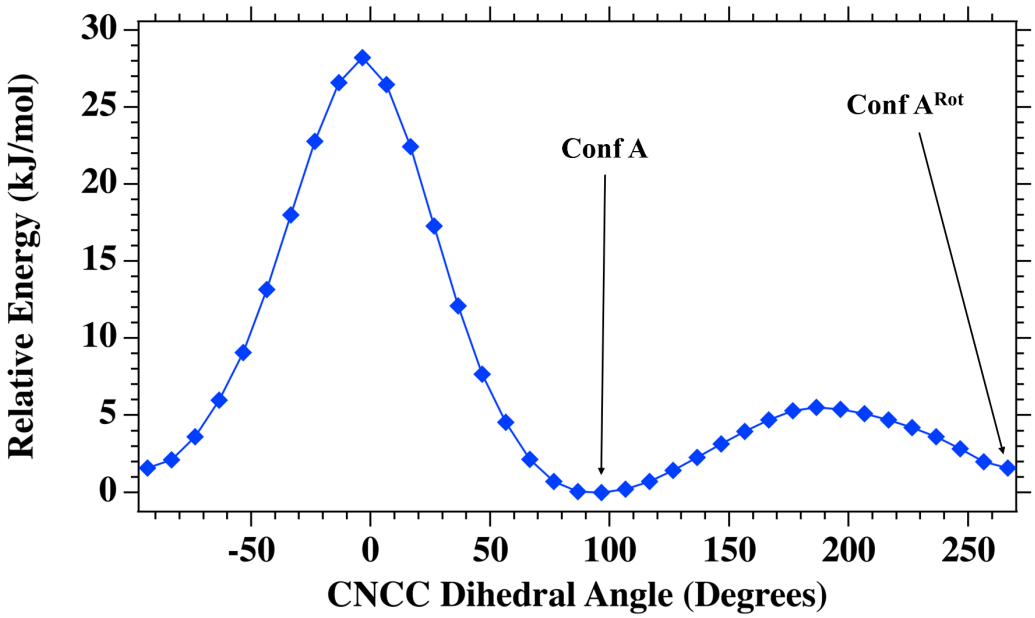

Figure S3: Relaxed potential energy scan about the relevant CNCC dihedral angle. The two rotameric minima are labelled, indicating where upon the potential energy surface they lie.

4. R2PI and IR-UV Holeburning Spectra of Ac-Ala-Asn-NHBn

The R2PI and IR-UV holeburning spectra for Ac-Ala-Asn-NHBn are presented in the top and bottom traces of **Figure S4**, respectively. The R2PI spectrum is dominated by an S_0-S_1 origin transition at 37,643 cm^{-1}. All vibronic transitions burn out in the IR-UV holeburning spectrum, demonstrating that only one conformer is present in the expansion. The spectrum has two vibronic peaks in a 61 cm^{-1} progression. Normal mode analysis of the assigned structure shows that this Franck-Condon active vibration is contributed to by modulation of the interior amide CNCC and by the twisting of the phenyl ring, the same twisting motion responsible for the 8 and 10 cm^{-1} progression in conformers A and B, respectively, of Ac-Asn-NHBn. Another two peaks in a 38 cm^{-1} progression are assigned to the rocking motion of the NHBn group against the acyl cap, during which the Asn NH_2 groups distance from the aromatic ring is modulated, consistent with inducing FC intensity via the ππ* transition. Finally, a single 88 cm^{-1} vibronic peak is due to the in-phase motion of the 38 cm^{-1} mode.

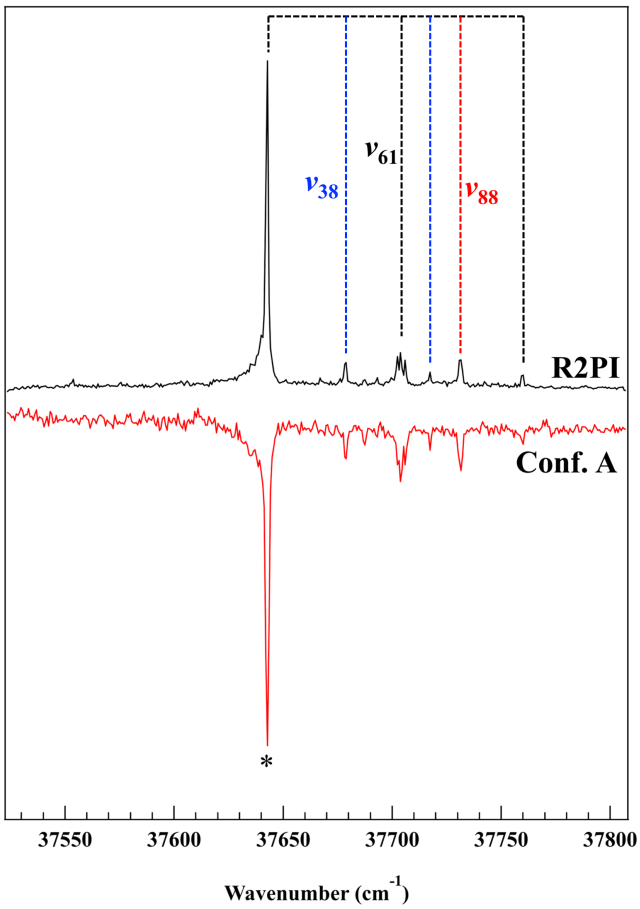

Figure S4: R2PI (black) and IR-UV holeburning (red) spectra of Ac-Ala-Asn-NHBn. The peak marked with an asterisk (37,643 cm^{-1}) indicates the transition used to collect RIDIR spectra. Vibronic progressions are labeled with tie lines.

5. R2PI and IR-UV Holeburning Spectra of Ac-Asn-Asn-NHBn

The R2PI and IR-UV holeburning spectra for Ac-Asn-Asn-NHBn are presented as the top and bottom trace of **Figure S5**, respectively. As with Ac-Ala-Asn-NHBn, the electronic spectrum is dominated by a single transition at 37,661 cm^{-1}. This $S_0 – S_1$ origin transition is located only 18 cm^{-1} higher in frequency than that of the Ala-containing analogue. This fact, combined with the general similarity of the R2PI spectra and their component RIDIR spectra indicate that the responsible conformers are structurally similar. All vibronic peaks burn out in the IR-UV holeburning spectra, proving that only one conformer is contributing to ultraviolet absorption in the expansion.

The vibronic band 30 cm^{-1} above the origin transition is assigned to a mode comprised of the NHBn rocking against the acyl cap, resulting in the C-terminal NH_2 group periodically modulating its distance from the aromatic ring. This is the analogous vibration to the 38 cm^{-1} Franck-Condon active mode in the R2PI spectrum of Ac-Ala-Asn-NHBn. The vibrational frequency is reduced by 8 cm^{-1} due to the increase in the reduced mass of the group vibration upon exchange of Ala for Asn (4.70 amu vs. 5.97 amu). The second most prominent vibronic peak is located 62 cm^{-1} from the origin transition. Normal mode analysis of the assigned structure reveals that the nuclear motion responsible is once again the modulation of the interior amide CNCC and the twisting of the phenyl ring, the same Franck-Condon active vibration in the R2PI spectra of Ac-Ala-Asn-NHBN.

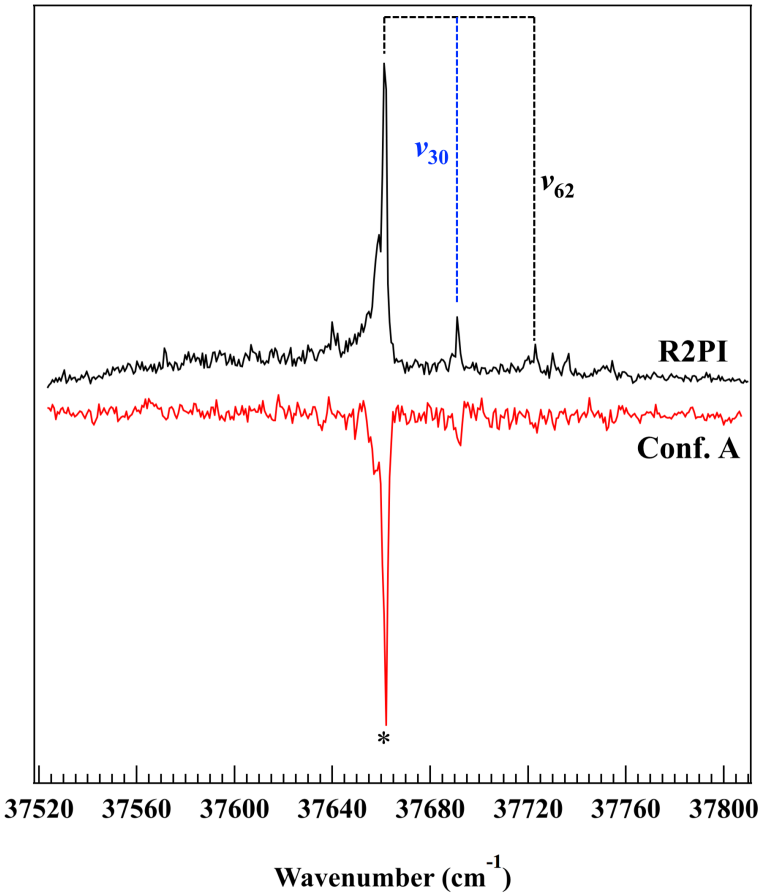

Figure S5: R2PI (black) and IR-UV holeburning (red) spectra of Ac-Asn-Asn-NHBn. The peak marked with an asterisk (37,662 cm^{-1}) indicates the transition used to collect RIDIR spectra. Vibronic progressions are labeled with tie lines.

6. Hydrogen Bonding Cycles, Calculated Distances, and Experimental Vibrational Frequencies for those Interactions Found in the Asn-Containing Peptides, Gln-Containing Peptides, and β-peptide Containing Foldamers

Table S1: Hydrogen bonding cycles, calculated distances, and experimental vibrational frequencies for those interactions found in the Asn-containing peptides studied in this work, compared with the analogous Gln-containing peptides studied previously, and foldamers incorporating β-amino acids which are able to form the same hydrogen bonded cycles as the Asn-containing peptides due to the number of carbon atoms between backbone amide groups.

Molecule	H-Bond Cycle	H-Bond Distance (Å)	Experimental Frequency (cm^{-1})
Ac-Asn-NHBn			
Conf A	$C7_{eq}$	1.90	3275
($C7_{eq}$//*C6/C7*)	*C6*	2.07	3357
	C7	2.15	3383 (3505)
Conf B	C5	2.15	3394
(C5//*C8/C7*)	*C8*	2.23	3353 (3510)
	C7	2.04	3279
Conf A^{Rot}	$C7_{eq}$	1.91	3279
($C7_{eq}$//*C6/C7*)	*C6*	2.09	3353
	C7	2.13	3394 (3310)
Ac-Gln-NHBn[a]			
Conf A	C5	2.11	3402
(C5//*C8*)	*C8*	1.96	3310
Conf B	C7	1.97	3354
(C7/π)	π		3415 (3529)
Conf C	$C7_{eq}$	1.92	3270
($C7_{eq}$//*C7/C8/π*)	*C7*	1.99	3343
	C8	2.24	3400 (3509)
Ac-Ala-Asn-NHBn			
Conf A	C10	1.99	3367
(C10//*C6/π*)	*C6*	2.08	3373
	π		3395 (3502)
Ac-Ala-Gln-NHBn[a]			
Conf A	C10	2.02	3357
(C10//*C7/π*)	*C7*	1.97	3361
	π		3408 (3520)
Ac-Asn-Asn-NHBn			
Conf A	C10	2.01	3350
(C10//*C6/C6/π*)	*C6*	2.16	3383
	C6	2.07	3359

	π		3393 (3505)
Ac-Gln-Gln-NHBn[b]	C		
Conf A	C10	1.99	3345
(C10//*C7/C7/π*)	*C7*	1.91	3324
	C7	1.98	3360
	π		3409 (3521)
Ac-β^3-hPhe-NHMe[c]			
C6	C6	2.08	3400
C8	C8	2.22	3412
Ac-β^3-hTyr-NHMe[c]			
C6	C6		3400
Ac-β$_{ACPC}$-L-Phe-NHMe[d]			
C8/C7$_{eq}$ (x3)	C8		3278, 3269, 3274
	C7$_{eq}$		3353, 3321, 3370
C11 (x2)	C11		3398,3412
Ac-L-Phe-β$_{ACPC}$- NHMe[d]			
C8/C5 (x2)	C8		3381,3383
	C5		3454,3450
Ac-β$_{ACPC}$ -D-Phe-NHMe[d]			
C8/C7$_{eq}$ (x4)	C8		3266, 3264, 3287, 3270
	C7$_{eq}$		3367, 3360, 3368, 3288
C11	C11		3374
Ac-β^3-hAla-L-Phe-NHMe[e]			
C8/C7$_{eq}$ (x3)	C8	2.20, 2.02, 1.96	3380, 3342, 3282
	C7$_{eq}$	2.19, 2.04, 2.06	3389, 3398, 3374
Ac-β^3-hAla-D-Phe-NHMe[e]			
C8/C7$_{eq}$ (x4)	C8	2.24, 2.04, 1.97, 1.96	3385, 3331, 3321, 3293
	C7$_{eq}$	2.23, 2.05, 2.02, 2.11	3373, 3357, 3365, 3390
Ac-L-Phe-β^3-hAla-NHMe[e]			
C8/C7$_{eq}$	C8	1.98	3399
	C7$_{eq}$	1.97	3314

[a]From ref. [1] [b]From ref. [2] [c]From ref. [3] [e]From ref. [4] [f]From ref. [5]

7. Backbone Overlap, and Hydride Stretch Comparison Spectra, of Ac-Ala-Asn-NHBn and Ac-Asn-Asn-NHBn

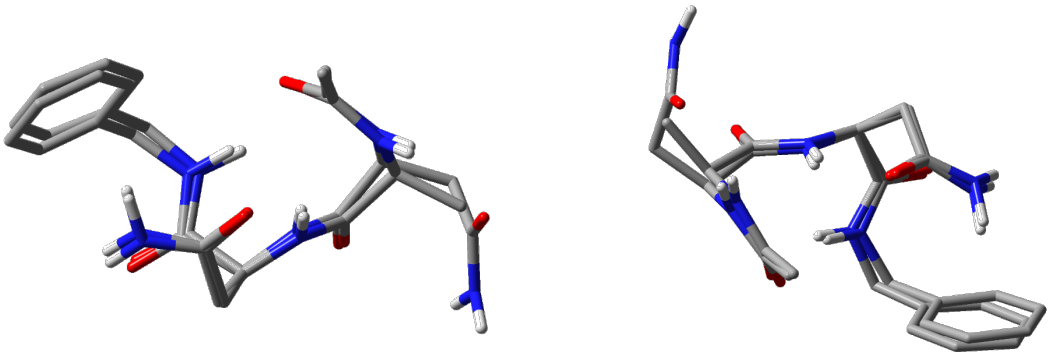

Figure S6: Two views of the peptide backbone overlap (with hydrogens removed) of Ac-Ala-Asn-NHBn and Ac-Asn-Asn-NHBn.

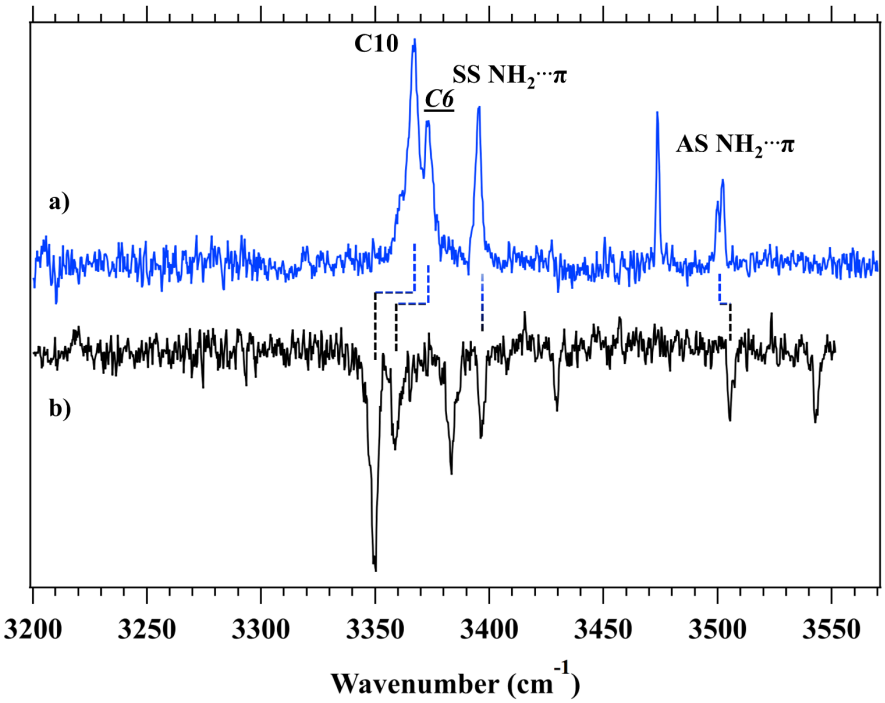

Figure S7: Experimental hydride stretch RIDIR spectra for the type I β-turn conformers of (a) Ac-Ala-Asn-NHBn and (b) Ac-Asn-Asn-NHBn. The shared spectral signatures of the two conformers are highlighted.

8. Backbone Overlap of Ac-Ala-Asn-NHBn and Ac-Ala-Gln-NHBn

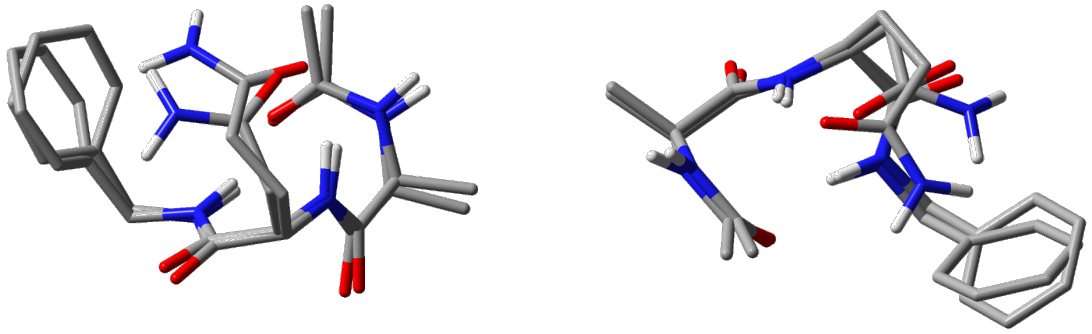

Figure S8: Two views of the peptide backbone overlap (with hydrogens removed) of Ac-Ala-Asn-NHBn and Ac-Ala-Gln-NHBn.

9. Backbone Overlap of Ac-Asn-Asn-NHBn and Ac-Gln-Gln-NHBn

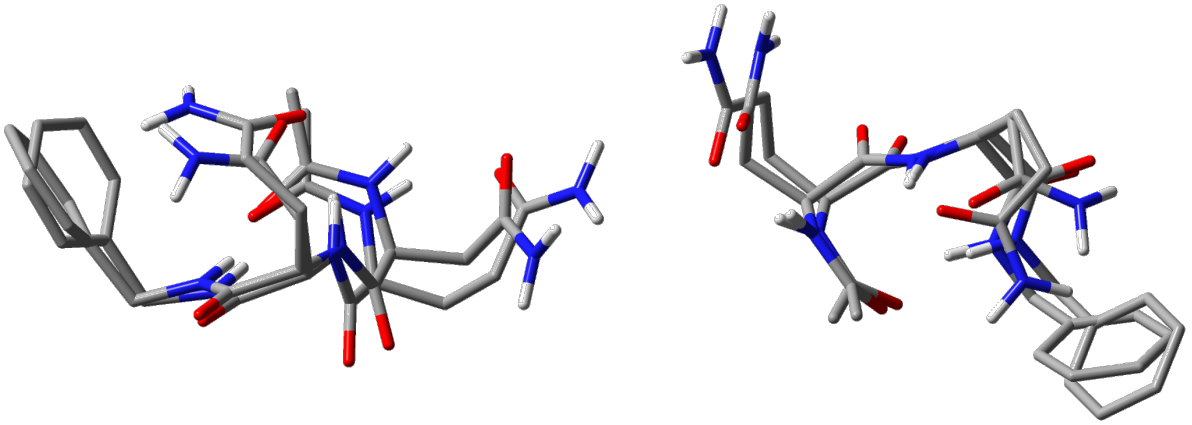

Figure S9: Two views of the peptide backbone overlap (with hydrogens removed) of Ac-Asn-Asn-NHBn and Ac-Gln-Gln-NHBn.

10. Free Energy Corrections for Ac-Asn-NHBn, Ac-Ala-Asn-NHBn, and Ac-Asn-Asn-NHBn

The nomenclature used in this section to describe conformational families is achieved by listing the hydrogen bonds as follows: backbone-backbone//sidechain-backbone//sidechain-sidechain, where each type of hydrogen bond is separated from the other by a double slash (//). If a designation begins with a double slash, it is implied that there are no backbone-backbone hydrogen bonds in the conformation being described. Bif is shorthand for bifurcated, describing a structure in which a single C=O is accepting hydrogen bonds from 2 NH donating groups.

Table S2: Relative potential energies, free energy corrections (at room temperature), and free energies for all calculated structures under 30 kJ/mol of the global energy minimum of Ac-Asn-NHBn, calculated at the DFT B3LYP-D3BJ/6-31+G(d)) level of theory. Note that experimentally assigned conformers A and B are the lowest calculated potential and free energy structures.

Ac-Asn-NHBn Conformer	**Conformational Family**	**ΔE (kJ/mol)**	**G correction (kJ/mol)**	**ΔG (kJ/mol)**
Conf A	**C7eq//C6/C7**	**0.0**	**0.0**	**0.0**
Conf A^{Rot}	C7eq//C6/C7	1.7	1.7	3.4
Conf B	**C5//C8/C7**	**2.1**	**1.1**	**3.2**
Phenyl ring rotamer of Conf B	C5//C8/C7	3.6	1.2	4.7
AcAsnNHBn_36.log:	//C6/pi	5.7	3.2	8.9
N_OPLS_34.log:	C7eq//C7	7.8	3.0	10.8
AcAsnNHBn_1.log:	C5//C7/pi	8.2	3.7	11.9
AcAsnNHBn_30.log:	//C6/C7	9.8	-2.0	7.8
AcAsnNHBn_13.log:	C7eq//C7	12.2	3.6	15.8
N_OPLS_4.log:	C7eq//C6	16.0	-2.3	13.6
AcAsnNHBn_46.log:	C7eq//C7	17.3	-4.2	13.1
AcAsnNHBn_42.log:	C5//C8/C7	17.4	0.8	18.1
AcAsnNHBn_7.log:	C7eq//C7	17.4	-2.2	15.3
N_OPLS_6.log:	C7eq//C6	18.3	-2.3	16.0
AcAsnNHBn_24.log:	C5//C8/C7	19.4	0.9	20.3
AcAsnNHBn_34.log:	C5//C8/C7	19.8	1.0	20.8
AcAsnNHBn_21.log:	C5//C8	20.5	1.7	22.2
N_OPLS_17.log:	//C6	20.7	-1.8	18.9
N_OPLS_12.log:	//C6	20.9	-1.4	19.5
N_OPLS_37.log:	C5//C8	21.9	-2.8	19.2

AcAsnNHBn_28.log:	C5//	22.0	-2.0	20.0
N_OPLS_9.log:	C7eq//	22.8	-4.1	18.7
N_OPLS_28.log:	//C6/pi	23.4	1.1	24.5
N_OPLS_7.log:	Bif C7ax-//-C8	24.0	4.5	28.6
AcAsnNHBn_12.log:	C7ax//pi	25.1	2.3	27.4
AcAsnNHBn_19.log:	C5//pi	25.3	1.7	26.9
AcAsnNHBn_39.log:	//C7/pi/C8	25.4	8.5	33.9
N_OPLS_43.log:	//C7	25.6	4.8	30.4
AcAsnNHBn_26.log:	C5//C7	25.8	-3.7	22.1
N_OPLS_31.log:	//C7	26.4	-1.8	24.6
AcAsnNHBn_47.log:	//C7	26.7	-0.5	26.1
N_OPLS_50.log:	BBifC5-//-C7	27.7	-2.6	25.1
AcAsnNHBn_29.log:	C7ax//C7	28.0	-2.6	25.3
AcAsnNHBn_37.log:	C7ax//C7	28.6	-1.4	27.1
N_OPLS_15.log:	C7ax//C7	28.6	-1.4	27.1

Table S3: Relative potential energies, free energy corrections (at room temperature), and free energies for all calculated structures under 30 kJ/mol of the global energy minimum of Ac-Ala-Asn-NHBn, calculated at the DFT B3LYP-D3BJ/6-31+G(d)) level of theory. Note that the experimentally assigned type I β-turn conformer remains the global minimum in both potential and free energy ranking.

Ac-Ala-Asn-NHBn Conformer	**Conformational Family**	**ΔE (kJ/mol)**	**G correction (kJ/mol)**	**ΔG (kJ/mol)**
Conf A (type I β-Turn)	**C10//C6/pi**	**0.0**	**0.0**	**0.0**
Ac-A-N_105.log:	C10//C6/C7	10.2	-7.4	2.8
AN_OPLS_29.log:	C7eq//C6/C7	13.4	-6.4	7.0
AN_OPLS_39.log:	C10//C6	15.7	-8.5	7.3
AN_OPLS_24.log:	C10//C6	17.5	-11.0	6.5
AN_OPLS_31.log:	C10//C6	18.4	-4.3	14.2
AcAlaAsnNHBn_98.log:	C7eq/C7eq//C7	18.5	-5.6	12.8
AcAlaAsnNHBn_99.log:	C7eq//C7/pi	19.2	-3.7	15.5
AN_OPLS_41.log:	C7eq//C7	20.4	-8.4	12.0
AN_OPLS_30.log:	Bif C5-C7eq//C6	21.6	-10.7	10.8
AN_OPLS_8.log:	C10//C7	22.1	-4.6	17.5
AN_OPLS_61.log:	C7eq//C6/C7	22.8	-11.1	11.7
AcAlaAsnNHBn_70.log:	C10//C7	23.3	-5.6	17.7
AN_OPLS_5.log:	C10	24.6	-4.4	20.2
AN_OPLS_47.log:	C7eq//C7	24.9	-10.3	14.6
AN_OPLS_7.log:	C7ax/pi/C7eq//C7	25.0	-3.4	21.7

AN_OPLS_19.log:	C7eq/C7eq//C7	25.8	-8.9	16.9
AcAlaAsnNHBn_62.log:	C5//C11	27.6	-9.5	18.2
Ac-A-N_113.log:	Bif C5-C7eq//C6/C7	28.9	-14.3	14.7
AN_OPLS_21.log:	C10//C8	29.1	-5.9	23.2
AcAlaAsnNHBn_56.log:	C5/C5//C8/C7	29.2	-15.2	14.1
AN_OPLS_3.log:	C7eq/pi/Bif C7ax-//-C8	29.3	-2.7	26.6
AN_OPLS_6.log:	C7eq/C7eq	29.6	-8.3	21.3

Table S4: Relative potential energies, free energy corrections (at room temperature), and free energies for all calculated structures under 30 kJ/mol of the global energy minimum of Ac-Asn-Asn-NHBn, calculated at the DFT B3LYP-D3BJ/6-31+G(d)) level of theory. Note that the experimentally assigned type I β-turn conformer remains the global minimum in both potential and free energy ranking.

Ac-Asn-Asn-NHBn Conformer	**Conformational Family**	**ΔE (kJ/mol)**	**G correction (kJ/mol)**	**ΔG (kJ/mol)**
Conf A (type I β-turn)	**C10//C6/C6/pi**	**0.0**	**0.0**	**0.0**
NN_OPLS_71.log:	C10//C6/C7//C11	6.8	9.7	16.5
Ac_NN_NHBn_AMBER_21.log:	C5//C8/C10/C6/pi	7.7	11.0	18.6
Ac_NN_NHBn_AMBER_47.log:	C5//C10/C6/pi	9.0	13.5	22.6
NN_OPLS_6.log:	C5//C10/pi/C6	15.8	13.0	28.8
Ac_NN_NHBn_AMBER_22.log:	C10//C7/pi/Bif C6-//-C11	17.8	16.4	34.2
NN_OPLS_109.log:	C10///C7//C11	18.1	8.8	26.9
NN_OPLS_83.log:	C5//C8/C10/C6	18.2	18.7	36.9
NN_OPLS_55.log:	C5//C8/C10/C6	19.5	8.4	27.9
NN_OPLS_77.log:	C10//Bif C6-//-C11	21.0	10.1	31.1
Ac_NN_NHBn_AMBER_35.log:	Bif C5-C7eq//C8/C7/C7	21.2	14.0	35.2
Ac_NN_NHBn_AMBER_13.log:	C5//C10/pi/C6	22.0	17.6	39.6
NN_OPLS_3.log:	Bif C5-C7eq//C7/pi/C7	23.2	11.7	35.0
Ac_NN_NHBn_AMBER_66.log:	Bif C5-C7eq//pi/C7/Bif C6-//C11	25.0	23.1	48.0

Ac_NN_NHBn_AMBER_44.log:	Bif C5-C7eq//C7/pi/C7	25.6	25.1	50.7
Ac_NN_NHBn_AMBER_19.log:	C5//Bif C7-C10/pi/C7	28.8	17.2	46.0
NN_OPLS_74.log:	C5//Bif C7-C10	28.8	14.9	43.7
Ac_NN_NHBn_AMBER_104.log:	Bif C5-C7eq//C7/pi	29.0	18.3	47.3
Ac_NN_NHBn_AMBER_53.log:	C7eq/Bif C7eq-//C7/pi/C7	29.5	22.3	51.7
Ac_NN_NHBn_AMBER_63.log:	C10//pi/C6	29.9	8.4	38.3
Ac_NN_NHBn_AMBER_97.log:	Bif C5-C7eq//C8/C7/C7	29.9	11.9	41.8
NN_OPLS_37.log:	C7eq//C7/C7/pi	30.0	14.7	44.7

11. Energetic Reordering upon Substitution of NHBn cap with NHMe cap with NHMe

The nomenclature used in this section to describe conformational families is achieved by listing the hydrogen bonds as follows: backbone-backbone//sidechain-backbone//sidechain-sidechain, where each type of hydrogen bond is separated from the other by a double slash (//). If a designation begins with a double slash, it is implied that there are no backbone-backbone hydrogen bonds in the conformation being described. Bif is shorthand for bifurcated, describing a structure in which a single C=O is accepting hydrogen bonds from 2 NH donating groups.

Table S5: Relative potential energies and conformational families of the 30 kJ/mol lowest energy structures of Ac-Asn-NHBn upon exchange of NHBn cap for NHMe cap and geometry optimization at the DFT B3LYP-D3BJ/6-31+G(d)) level of theory. Note that for the two observed conformers both the energy ordering and conformational family remain the same upon NHMe substitution.

Ac-Asn-NHBn Conformer	**NHBn Conformational Family**	**ΔE (kJ/mol) (NHBn cap)**	**NHMe Conformational Family**	**ΔE (kJ/mol) (NHMe cap)**
Conf A	**C7eq//C6/C7**	**0.0**	**C7eq//C6/C7**	**0.0**
Conf A^{Rot}	C7eq//C6/C7	1.7	C7eq//C6/C7	0.0
Conf B	**C5//C8/C7**	**2.1**	**C5//C8/C7**	**2.0**

Phenyl ring rotamer of Conf B	C5//C8/C7	3.6	C5//C8/C7	2.0
AcAsnNHBn_36.log:	//C6/pi	5.7	C7eq//C6/C7	0.0
N_OPLS_34.log:	C7eq//C7	7.8	C7eq//C6/C7	0.0
AcAsnNHBn_1.log:	C5//C7/pi	8.2	C5//C8/C7	2.0
AcAsnNHBn_30.log:	//C6/C7	9.8	C7eq//C6/C7	0.0
AcAsnNHBn_13.log:	C7eq//C7	12.2	//C7/C7	15.5
N_OPLS_4.log:	C7eq//C6	16.0	C7eq//C6	16.9
AcAsnNHBn_46.log:	C7eq//C7	17.3	//C7/C7	15.5
AcAsnNHBn_42.log:	C5//C8/C7	17.4	C5//C8/C7	16.7
AcAsnNHBn_7.log:	C7eq//C7	17.4	//C7/C7	15.5
N_OPLS_6.log:	C7eq//C6	18.3	C7eq//C6	16.9
AcAsnNHBn_24.log:	C5//C8/C7	19.4	C5//C8/C7	16.7
AcAsnNHBn_34.log:	C5//C8/C7	19.8	C5//C8/C7	16.7
AcAsnNHBn_21.log:	C5//C8	20.5	C5//C8/C7	16.7
N_OPLS_17.log:	//C6	20.7	//C6	25.9
N_OPLS_12.log:	//C6	20.9	//C6	25.6
N_OPLS_37.log:	C5//C8	21.9	C7ax//C7	21.3
AcAsnNHBn_28.log:	C5//	22.0	C5//C7	23.9
N_OPLS_9.log:	C7eq//	22.8	C7ax	23.8
N_OPLS_28.log:	//C6/pi	23.4	C7eq//C6/C7	0.0
N_OPLS_7.log:	Bif C7ax-//-C8	24.0	C7ax	24.9
AcAsnNHBn_12.log:	C7ax//pi	25.1	C7ax	35.5
AcAsnNHBn_19.log:	C5//pi	25.3	C7eq//C6/C7	0.0
AcAsnNHBn_39.log:	//C7/pi/C8	25.4	//C8/C7	34.5
N_OPLS_43.log:	//C7	25.6	//C7	29.9
AcAsnNHBn_26.log:	C5//C7	25.8	C5//C7	23.9
N_OPLS_31.log:	//C7	26.4	//C7	30.1
AcAsnNHBn_47.log:	//C7	26.7	//C7	32.2
N_OPLS_50.log:	Bif C5-//-C7	27.7	C7eq//C6/C7	0.0
AcAsnNHBn_29.log:	C7ax//C7	28.0	C7ax//C7	28.5
AcAsnNHBn_37.log:	C7ax//C7	28.6	C7ax//C7	28.5
N_OPLS_15.log:	C7ax//C7	28.6	C7ax//C7	28.5

Table S6: Relative potential energies and conformational families of the 30 kJ/mol lowest energy structures of Ac-Ala-Asn-NHBn upon exchange of NHBn cap for NHMe cap and geometry optimization at the DFT B3LYP-D3BJ/6-31+G(d)) level of theory. Note that the experimentally observed conformer remains the global energy minimum. Also, the type I β-turn structure is conserved even without the π interaction with the NHBn cap.

Ac-Ala-Asn-NHBn Conformer	**NHBn Conformational Family**	**ΔE (kJ/mol) (NHBn cap)**	**NHMe Conformational Family**	**ΔE (kJ/mol) (NHMe cap)**
Conf A (type I β-turn)	**C10//C6/pi**	**0.0**	**C10//C6**	**0.0**
Ac-A-N_105.log:	C10//C6/C7	10.2	C10//C6	0.0
AN_OPLS_29.log:	C7eq//C6/C7	13.4	C7eq//C6/C7	4.6
AN_OPLS_39.log:	C10//C6	15.7	C10//C6	0.0
AN_OPLS_24.log:	C10//C6	17.5	C10//C6	0.0
AN_OPLS_31.log:	C10//C6	18.4	C10//C6/C7	10.7
AcAlaAsnNHBn_98.log:	C7eq/C7eq//C7	18.5	C7eq/C7eq//C7	9.8
AcAlaAsnNHBn_99.log:	C7eq//C7/pi	19.2	C7eq//C7	7.5
AN_OPLS_41.log:	C7eq//C7	20.4	C7eq//C7	7.5
AN_OPLS_30.log:	Bif C5-C7eq//C6	21.6	Bif C5-C7eq//C6/C7	10.7
AN_OPLS_8.log:	C10//C7	22.1	C10//C7	22.3
AN_OPLS_61.log:	C7eq//C6/C7	22.8	C7eq//C6/C7	4.6
AcAlaAsnNHBn_70.log:	C10//C7	23.3	C10//C7	22.3
AN_OPLS_5.log:	C10	24.6	C10//C8	24.3
AN_OPLS_47.log:	C7eq//C7	24.9	C7eq//C7	7.5
AN_OPLS_7.log:	C7ax/pi/C7eq//C7	25.0	C7ax/C7eq//C7	24.9
AN_OPLS_19.log:	C7eq/C7eq//C7	25.8	C7eq/C7eq//C7	15.8
AcAlaAsnNHBn_62.log:	C5//C11	27.6	C5//C11/C7	13.1
Ac-A-N_113.log:	Bif C5-C7eq//C6/C7	28.9	Bif C5-C7eq//C6/C7	10.7
AN_OPLS_21.log:	C10//C8	29.1	C10//C8	22.3
AcAlaAsnNHBn_56.log:	C5/C5//C8/C7	29.2	C5/C5//C8/C7	12.4
AN_OPLS_3.log:	C7eq/pi/Bif C7ax-//-C8	29.3	C7eq/Bif C7ax-//-C8	29.0
AN_OPLS_6.log:	C7eq/C7eq	29.6	C7eq/C7eq	15.1

Table S7: Relative potential energies and conformational families of the 30 kJ/mol lowest energy structures of Ac-Asn-Asn-NHBn upon exchange of NHBn cap for NHMe cap and geometry optimization at the DFT B3LYP-D3BJ/6-31+G(d)) level of theory. Note that the experimentally observed conformer moves from the lowest to the second lowest energy structure upon NHMe cap substitution. The conformer that moved to the global minimum position is also a type I β-turn which differentiates itself from the experimentally observed structure by having a sidechain-sidechain hydrogen bond.

Ac-Asn-Asn-NHBn Conformer	**NHBn Conformational Family**	**ΔE (kJ/mol) (NHBn cap)**	**NHMe Conformational Family**	**ΔE (kJ/mol) (NHMe cap)**
Conf A (type I β-turn)	**C10//C6/C6/pi**	**0.0**	**C10//C6/C6**	**0.6**
NN_OPLS_71.log:	C10//C6/C7//C11	6.8	C10//C6/C7//C11	0.0
Ac_NN_NHBn_AMBER_21.log:	C5//C8/C10/C6/pi	7.7	C5//C8/C10/C6	6.4
Ac_NN_NHBn_AMBER_47.log:	C5//C10/C6/pi	9.0	C5//C8/C10/C6	6.4
NN_OPLS_6.log:	C5//C10/pi/C6	15.8	C5//C8/C10/C6	6.4
Ac_NN_NHBn_AMBER_22.log:	C10//C7/pi/Bif C6-//-C11	17.8	C10//C7/Bif C6-//-C11	14.7
NN_OPLS_109.log:	C10///C7//C11	18.1	C10//C7//C11	14.4
NN_OPLS_83.log:	C5//C8/C10/C6	18.2	C5//C8/C10/C6/C6	3.6
NN_OPLS_55.log:	C5//C8/C10/C6	19.5	C5//C8/C10/C6	6.4
NN_OPLS_77.log:	C10//Bif C6-//-C11	21.0	C10//C7/Bif C6-//-C11	14.7
Ac_NN_NHBn_AMBER_35.log:	BifC5-C7eq//C8/C7/C7	21.2	Bif C5-C7eq//C8/C7/C7	16.7
Ac_NN_NHBn_AMBER_13.log:	C5//C10/pi/C6	22.0	C5//C8/C10/C6	6.4
NN_OPLS_3.log:	Bif C5-C7eq//C7/pi/C7	23.2	Bif C5-C7eq//C8/C7/C7	16.7
Ac_NN_NHBn_AMBER_66.log:	BifC5-C7eq//pi/C7/BifC6-//C11	25.0	Bif C5-C7eq//Bif C6-//C11	16.3
Ac_NN_NHBn_AMBER_44.log:	Bif C5-C7eq//C7/pi/C7	25.6	BifC5-C7eq//C8/C7/C7	18.2

Ac_NN_NHBn_AMBER_19.log:	C5//Bif C7-C10/pi/C7	28.8	C5//C8/Bif C7-C10/C7	19.2
NN_OPLS_74.log:	C5//Bif C7-C10	28.8	C5//C8/Bif C7-C10/C7	19.1
Ac_NN_NHBn_AMBER_104.log:	Bif C5-C7eq//C7/pi	29.0	Bif C5-C7eq//C8/BifC7-//C11	18.1
Ac_NN_NHBn_AMBER_53.log:	C7eq/Bif C7eq-//C7/pi/C7	29.5	C7eq/Bif C7eq-//-C7/C7	31.2
Ac_NN_NHBn_AMBER_63.log:	C10//pi/C6	29.9	C10//C7/Bif C6-//-C11	14.7
Ac_NN_NHBn_AMBER_97.log:	Bif C5-C7eq//C8/C7/C7	29.9	Bif C5-C7eq//C8/C7/C7	31.1
NN_OPLS_37.log:	C7eq//C7/C7/pi	30.0	C7eq//C7/C7	18.1

12. Figure S10: Comparison of NHBn and NHMe capped Ac-Asn-Asn-NHBn Conf A and Calculated Low Energy C10//*C6/C7*//C11 Structures

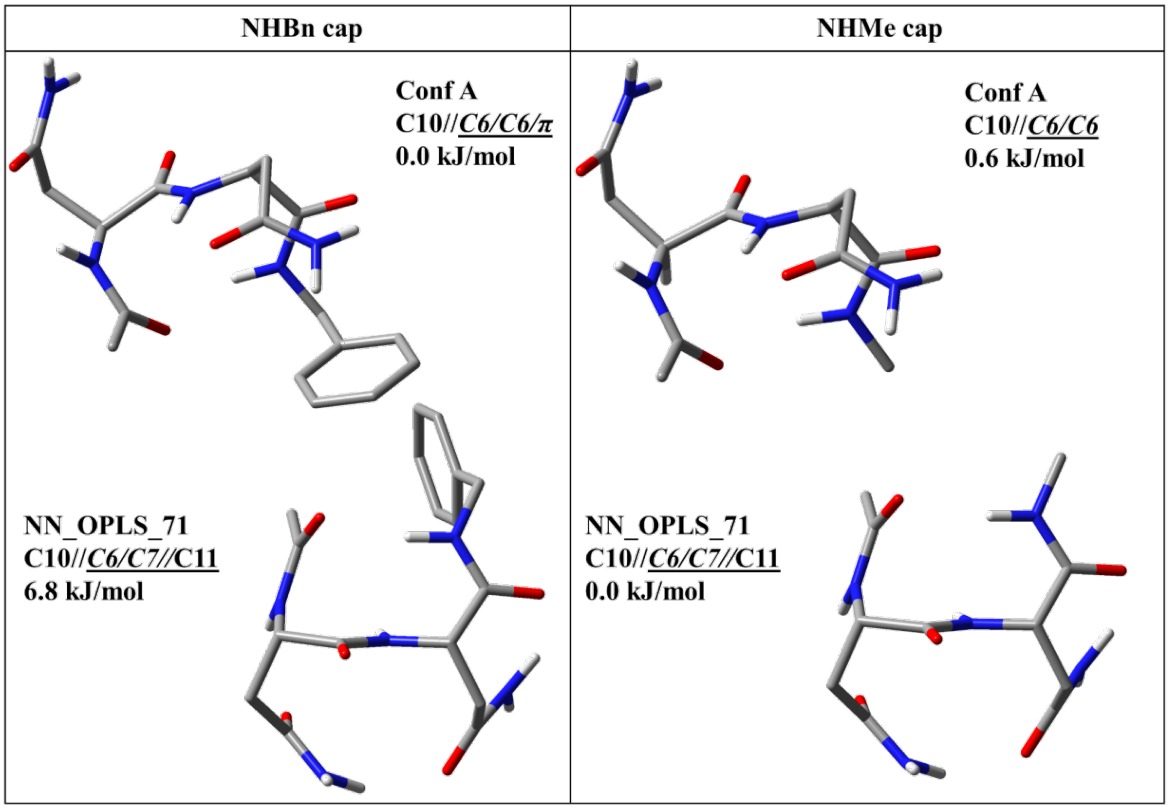

Figure S10: Comparison of the assigned type I β-turn structure of Ac-Asn-Asn-NHBn with the second lowest energy calculated structure which engages in sidechain-sidechain hydrogen bonding. Structures and energies are displayed for both NHBn and NHMe caps. Note that the energy ordering flips upon cap substitution.

13. Comparison of type I β-turn Dihedral Angles of Assigned Dipeptides with Those Found in the Protein Data Bank with Sequence X(AN)X And X(NN)X

Table **S8:** Ramachandran angle comparison of type I β-turns with sequence X(NN)X

			Turn residues	
Structure	Turn sequence	Residue #	(*i+1*) (phi,psi) (degrees)	(*i+2*) (phi,psi) (degrees)
Ac-N-N-NHBn[a]	X(NN)X		-75.8, 0.9	-83.4, -2.7
Chromosome condensation regulator[b]	D(NN)G	148-151	-63.7,-23.8	-100.6, 0
Tetanus toxin C fragment[c]	Q(NN)Q	216-219	-55.0, -19.6	-105.7, 5.8
Human aldose reductase holoenzyme[d]	L(NN)G	6-9	-71.6, -8.4	-96.9, 8.7
Rat pancreatic lipase protein[e]	G(NN)G Z	361-364	-68.6, -16.3	-93.7, -6.8
Staphopain, cysteine proteinase[f]	L(NN)G	130-133	-59.7, -24.3	-93.0, 10.8
Galactose oxidase[g]	R(NN)W	11-14	-49.3, -66.6	-70.2, -2.8
Bacterial cellulose-binding domain[h]	T(NN)A	85-88	-69.1, -11.2	-129.6, 19.1
Human cytomegalovirus DNA polymerase subunit[i]	S(NN)R	205-208	-55.1, -40.8	-79.0, 10.4
Vaccinia virus DNA topoisomerase I[j]	D(NN)F	14-17	-71.7, -9.0	-95.4, -3.2
Recombinant apo-chloroperoxidase[k]	D(NN)G	520-523	-57.2, -29.1	-95.1, -0.1
Average of crystal structures	X(NN)X		-62.1, -24.9	-95.9, 4.2

[a] This work. [b] (PDB ID: 1a12).[6] [c] (PDB ID: 1a8d).[7] [d] (PDB ID: 1ads).[8] [e] (PDB ID: 1bu8).[9] [f] (PDB ID: 1cv8).[10] [g] (PDB ID: 1gof).[11] [h] (PDB ID: 1nbc).[12] [i] (PDB ID: 1t6l).[13] [j] (PDB ID: 1vcc). [14] [k] (PDB ID: 1vns).[15]

Table **S9:** Ramachandran angle comparison of type I β-turns with sequence X(AN)X

			Turn residues	
Structure	Turn sequence/residue #	Residue #	(*i+1*) (phi,psi) (degrees)	(*i+2*) (phi,psi) (degrees)
Ac-A-N-NHBn[a]	X(AN)X		-68.1, -13.0	-80.0, -0.5
Sulfate reductase[b]	T(AN)Q	393-396	-75.0, -6.1	-104.1, 20.4
Mutant H42Q of hipip[c]	P(AN)A	3-6	-66.7, -21.3	-103.1, 24.5
Beta-mannanase[d]	E(AN)G	13-16	-57.4, -31.6	-77.9, 1.9
Electron transport protein[e]	P(AN)L	96-99	-71.7, -20.5	-100.9, 12.6
Type II activin receptor extracellular domain[f]	N(AN)W	15-18	-63.8, -21.4	-96.0, 27.4
Phenylalanine dehydrogenase[g]	V(AN)A	286-289	-61.6, -36.7	-97.7, 12
Endoglucanase A catalytic core[h]	D(AN)N	135-138	-65.1, -13.6	-97.7, 7.9
3-Isopropylmalate dehydrogenase[i]	K(AN)V	195-198	-71.9, -10.5	-75.4, -13.1
Cystathionine gamma-synthase[j]	A(AN)K	382-385	-66.9, -29.6	-89.6, 22.7
Bacterial lipase[k]	G(AN)A	297-300	-57.7, -26.9	-94.6, -2.6
Deacetyoxycephalosporin C synthase[l]	C(AN)G	197-200	-57.4, -35.7	-84.2, 3.9
Celcca catalytic domain[m]	F(AN)Y	156-159	-54.2, -32.8	-86.9, -4.3
DD-transpeptidase mutant[n]	V(AN)N	68-71	-64.3, -29.9	-106.4, 6.6
Pseudomonas aeruginosa elastase[o]	L(AN)S	236-239	-62.2, -25.5	-99.2, 11.3
Serine protease[p]	Y(AN)A	171-174	-57.3, -37.6	-87.9, 13.3
Leucine aminopeptidase[q]	P(AN)E	174-177	-58.9, -26.5	-71.1, -19.2
Deubiquitinating enzyme[r]	I(AN)N	104-107	-53.0, -38.0	-89.6, 8.4
Average of crystal structures	X(AN)X		-62.7, -26.1	-91.9, 7.9

[a] This work. [b] (PDB ID: 1aop).[16] [c] (PDB ID: 1b0y).[17] [d] (PDB ID: 1bqc).[18] [e] (PDB ID: 1bqk).[19] [f] (PDB ID: 1bte).[20] [g] (PDB ID: 1bw9).[21] [h] (PDB ID: 1cem).[22] [i] (PDB ID: 1cnz).[23] [j] (PDB ID: 1cs1).[24] [k] (PDB ID: 1cvl).[25] [l] (PDB ID: 1dcs).[26] [m] (PDB ID: 1edg).[27] [n] (PDB ID: 1es5).[28] [o] (PDB ID: 1ezm).[29] [p] (PDB ID: 1GCI).[30] [q] (PDB ID: 1lam).[31] [r] (PDB ID: 1uch).[32]

14. References

1. Walsh, P. S.; Dean, J. C.; McBurney, C.; Kang, H.; Gellman, S. H.; Zwier, T. S., Conformation-Specific Spectroscopy of Capped Glutamine-Containing Peptides: Role of a Single Glutamine Residue on Peptide Backbone Preferences. *PCCP* **2016,** *18* (16), 11306-11322.
2. Walsh, P. S.; Blodgett, K. N.; McBurney, C.; Gellman, S. H.; Zwier, T. S., Inherent Conformational Preferences of Ac-Gln-Gln-Nhbn: Sidechain Hydrogen Bonding Supports a B-Turn in the Gas Phase. *Angew. Chem. Int. Ed.* **2016,** *55* (47), 14618-14622.
3. Baquero, E. E.; James, W. H.; Choi, S. H.; Gellman, S. H.; Zwier, T. S., Single-Conformation Ultraviolet and Infrared Spectroscopy of Model Synthetic Foldamers: B-Peptides Ac-B3-Hphe-Nhme and Ac-B3-Htyr-Nhme. *J. Am. Chem. Soc.* **2008,** *130* (14), 4784-4794.
4. James, W. H.; Baquero, E. E.; Choi, S. H.; Gellman, S. H.; Zwier, T. S., Laser Spectroscopy of Conformationally Constrained A/B-Peptides: Ac-Acpc-Phe-Nhme and Ac-Phe-Acpc-Nhme. *J. Phys. Chem. A* **2010,** *114* (3), 1581-1591.
5. James, W. H.; Baquero, E. E.; Shubert, V. A.; Choi, S. H.; Gellman, S. H.; Zwier, T. S., Single-Conformation and Diastereomer Specific Ultraviolet and Infrared Spectroscopy of Model Synthetic Foldamers: A/B-Peptides. *J. Am. Chem. Soc.* **2009,** *131* (18), 6574-6590.
6. Renault, L.; Nassar, N.; Vetter, I.; Becker, J.; Klebe, C.; Roth, M.; Wittinghofer, A., The 1.7 Å Crystal Structure of the Regulator of Chromosome Condensation (Rcc1) Reveals a Seven-Bladed Propeller. *Nature* **1998,** *392*, 97.
7. Knapp, M., Segelke, B., Rupp, B., The 1.61 Angstrom Structure of the Tetanus Toxin Ganglioside Binding Region: Solved by Mad and Mir Phase Combination. *Am.Cryst.Assoc.,Abstr.Papers (Annual Meeting)* **1998,** *25* (90).
8. Wilson, D.; Bohren, K.; Gabbay, K.; Quiocho, F., An Unlikely Sugar Substrate Site in the 1.65 a Structure of the Human Aldose Reductase Holoenzyme Implicated in Diabetic Complications. *Science* **1992,** *257* (5066), 81-84.
9. Roussel, A.; Yang, Y.; Ferrato, F.; Verger, R.; Cambillau, C.; Lowe, M., Structure and Activity of Rat Pancreatic Lipase-Related Protein 2. *J. Biol. Chem.* **1998,** *273* (48), 32121-32128.
10. Hofmann, B.; Schomburg, D.; Hecht, H., Crystal Structure of a Thiol Proteinase from Staphylococcus Aureus V-8 in the E-64 Inhibitor Complex. *Acta Crystallogr.* **1993,** *49* (Suppl), 102.
11. Ito, N.; Phillips, S. E.; Stevens, C.; Ogel, Z. B.; McPherson, M. J.; Keen, J. N.; Yadav, K. D.; Knowles, P. F., Novel Thioether Bond Revealed by a 1.7 Å Crystal Structure of Galactose Oxidase. *Nature* **1991,** *350* (6313), 87-90.
12. Tormo, J.; Lamed, R.; Chirino, A. J.; Morag, E.; Bayer, E. A.; Shoham, Y.; Steitz, T. A., Crystal Structure of a Bacterial Family-Iii Cellulose-Binding Domain: A General Mechanism for Attachment to Cellulose. *The EMBO journal* **1996,** *15* (21), 5739.
13. Appleton, B. A.; Loregian, A.; Filman, D. J.; Coen, D. M.; Hogle, J. M., The Cytomegalovirus DNA Polymerase Subunit Ul44 Forms a C Clamp-Shaped Dimer. *Mol. Cell* **2004,** *15* (2), 233-244.
14. Sharma, A.; Hanai, R.; Mondragón, A., Crystal Structure of the Amino-Terminal Fragment of Vaccinia Virus DNA Topoisomerase I at 1.6 Å Resolution. *Structure* **1994,** *2* (8), 767-777.

15. Macedo-Ribeiro, S.; Hemrika, W.; Renirie, R.; Wever, R.; Messerschmidt, A., X-Ray Crystal Structures of Active Site Mutants of the Vanadium-Containing Chloroperoxidase from the Fungus Curvularia Inaequalis. *J. Biol. Inorg. Chem.* **1999,** *4* (2), 209-219.
16. Crane, B. R.; Siegel, L. M.; Getzoff, E. D., 1.6 A: Evolution and Catalysis for Reduction of Inorganic Anions. *Science* **1995,** *270*, 59.
17. Parisini, E.; Capozzi, F.; Lubini, P.; Lamzin, V.; Luchinat, C.; Sheldrick, G. M., Ab Initio Solution and Refinement of Two High-Potential Iron Protein Structures at Atomic Resolution. *Acta Crystallogr. Sect. D. Biol. Crystallogr.* **1999,** *55* (11), 1773-1784.
18. Hilge, M.; Gloor, S. M.; Rypniewski, W.; Sauer, O.; Heightman, T. D.; Zimmermann, W.; Winterhalter, K.; Piontek, K., High-Resolution Native and Complex Structures of Thermostable B-Mannanase from Thermomonospora Fusca–Substrate Specificity in Glycosyl Hydrolase Family 5. *Structure* **1998,** *6* (11), 1433-1444.
19. Inoue, T.; Nishio, N.; Suzuki, S.; Kataoka, K.; Kohzuma, T.; Kai, Y., Crystal Structure Determinations of Oxidized and Reduced Pseudoazurins from Achromobacter Cycloclastes Concerted Movement of Copper Site in Redox Forms with the Rearrangement of Hydrogen Bond at a Remote Histidine. *J. Biol. Chem.* **1999,** *274* (25), 17845-17852.
20. Greenwald, J.; Fischer, W. H.; Vale, W. W.; Choe, S., Three-Finger Toxin Fold for the Extracellular Ligand-Binding Domain of the Type Ii Activin Receptor Serine Kinase. *Nat. Struct. Mol. Biol.* **1999,** *6* (1), 18-22.
21. Vanhooke, J. L.; Thoden, J. B.; Brunhuber, N. M.; Blanchard, J. S.; Holden, H. M., Phenylalanine Dehydrogenase from Rhodococcus Sp. M4: High-Resolution X-Ray Analyses of Inhibitory Ternary Complexes Reveal Key Features in the Oxidative Deamination Mechanism. *Biochem. (Mosc.)* **1999,** *38* (8), 2326-2339.
22. Alzari, P. M.; ne Souchon, H.; Dominguez, R., The Crystal Structure of Endoglucanase Cela, a Family 8 Glycosyl Hydrolase from Clostridium Thermocellum. *Structure* **1996,** *4* (3), 265-275.
23. Wallon, G.; Kryger, G.; Lovett, S. T.; Oshima, T.; Ringe, D.; Petsko, G. A., Crystal Structures of Escherichia Coli and Salmonella Typhimurium 3-Isopropylmalate Dehydrogenase and Comparison with Their Thermophilic Counterpart from Thermus Thermophilus. *J. Mol. Biol.* **1997,** *266* (5), 1016-1031.
24. Clausen, T.; Huber, R.; Prade, L.; Wahl, M. C.; Messerschmidt, A., Crystal Structure of Escherichia Coli Cystathionine Γ-Synthase at 1.5 Å Resolution. *The EMBO journal* **1998,** *17* (23), 6827-6838.
25. Lang, D.; Hofmann, B.; Haalck, L.; Hecht, H.-J.; Spener, F.; Schmid, R. D.; Schomburg, D., Crystal Structure of a Bacterial Lipase Fromchromobacterium Viscosumatcc 6918 Refined at 1.6 Å Resolution. *J. Mol. Biol.* **1996,** *259* (4), 704-717.
26. Valegård, K.; van Scheltinga, A. C. T.; Lloyd, M. D.; Hara, T.; Ramaswamy, S.; Perrakis, A.; Thompson, A.; Lee, H.-J.; Baldwin, J. E.; Schofield, C. J., Structure of a Cephalosporin Synthase. *Nature* **1998,** *394* (6695), 805-809.
27. Ducros, V.; Czjzek, M.; Belaich, A.; Gaudin, C.; Fierobe, H.-P.; Belaich, J.-P.; Davies, G. J.; Haser, R., Crystal Structure of the Catalytic Domain of a Bacterial Cellulase Belonging to Family 5. *Structure* **1995,** *3* (9), 939-949.
28. Fonze, E., Rhazi, N., Nguyen-Disteche, M., Charlier, P., Dd-Transpeptidase. *To be published* **2000**.

29. Thayer, M.; Flaherty, K. M.; McKay, D. B., Three-Dimensional Structure of the Elastase of Pseudomonas Aeruginosa at 1.5-a Resolution. *J. Biol. Chem.* **1991,** *266* (5), 2864-2871.
30. Kuhn, P.; Knapp, M.; Soltis, S. M.; Ganshaw, G.; Thoene, M.; Bott, R., The 0.78 Å Structure of a Serine Protease: Bacillus Lentus Subtilisin. *Biochem. (Mosc.)* **1998,** *37* (39), 13446-13452.
31. Straeter, N.; Lipscomb, W. N., Two-Metal Ion Mechanism of Bovine Lens Leucine Aminopeptidase: Active Site Solvent Structure and Binding Mode of L-Leucinal, a Gem-Diolate Transition State Analog, by X-Ray Crystallography. *Biochem. (Mosc.)* **1995,** *34* (45), 14792-14800.
32. Johnston, S. C.; Larsen, C. N.; Cook, W. J.; Wilkinson, K. D.; Hill, C. P., Crystal Structure of a Deubiquitinating Enzyme (Human Uch-L3) at 1.8 Å Resolution. *The EMBO Journal* **1997,** *16* (13), 3787-3796.